The American Journal of Pathology, Vol. 175, No. 4, October 2009

DOI: 10.2353/ajpath.2009.090133

Vascular Biology, Atherosclerosis and Endothelium Biology

Role of CD11b$^+$ Macrophages in Intraperitoneal Lipopolysaccharide-Induced Aberrant Lymphangiogenesis and Lymphatic Function in the Diaphragm

Kyung Eun Kim,* Young-Jun Koh,* Bong-Hyun Jeon,* Cholsoon Jang,* Jinah Han,* Raghu P. Kataru,* Reto A. Schwendener,† Jin-Man Kim,‡ and Gou Young Koh*

From the National Research Laboratory of Vascular Biology and Department of Biological Sciences and Graduate School of Nanoscience and Technology (World Class University), Korea Advanced Institute of Science and Technology, Daejeon, Korea; the Laboratory of Liposome Research,† Institute of Molecular Cancer Research, University of Zurich, Zurich, Switzerland; and the Department of Pathology,‡ Chungnam National University School of Medicine, Daejeon, Korea*

Lymphatic vessels in the diaphragm are essential for draining peritoneal fluid, but little is known about their pathological changes during inflammation. Here we characterized diaphragmatic lymphatic vessels in a peritonitis model generated by daily i.p. administration of lipopolysaccharide (LPS) in mice. Intraperitoneal LPS increased lymphatic density, branching, sprouts, connections, and network formation in the diaphragm in time- and dose-dependent manners. These changes were reversible on discontinuation of LPS administration. The LPS-induced lymphatic density and remodeling occur mainly through proliferation of lymphatic endothelial cells. CD11b$^+$ macrophages were massively accumulated and closely associated with the lymphatic vessels changed by i.p. LPS. Both RT-PCR assays and experiments with vascular endothelial growth factor-C/D blockade and macrophage-depletion indicated that the CD11b$^+$ macrophage-derived lymphangiogenic factors vascular endothelial growth factor-C/D could be major mediators of LPS-induced lymphangiogenesis and lymphatic remodeling through paracrine activity. Functional assays with India ink and fluorescein isothiocyanate-microspheres indicated that impaired peritoneal fluid drainage in diaphragm of LPS-induced peritonitis mice was due to inflammatory fibrosis and massive attachment of CD11b$^+$ macrophages on the peritoneal side of the diaphragmatic lymphatic vessels. These findings reveal that CD11b$^+$ macrophages play an important role in i.p. LPS-induced aberrant lymphangiogenesis and lymphatic dysfunction in the diaphragm. ***(Am J Pathol 2009, 175:1733–1745; DOI: 10.2353/ajpath.2009.090133)***

The peritoneum provides the lining of the peritoneal cavity and is the most extensive serous membrane in the body.[1] The peritoneal membrane is formed by a single layer of mesothelial cells. Beneath the mesothelial cells, there is a very thin and discontinuous layer of connective tissue and a layer of fenestrated lymphatic vessels.[2] These three layers not only function as an absorptive surface for peritoneal fluid but also remove pathogens and prevent cells from leaking through damage in the gastrointestinal tract or ascending through the female genital tract.[3,4] The peritoneum also plays crucial roles in the local defensive response against bacterial invasion with appropriate activation of resident immune cells and the recruitment of circulating immune cells.[5,6]

Lymphatic vessels have distinctive morphologies and functions in different tissues and organs.[7,8] Lymphatic vessels play an essential role in the maintenance of tissue fluid homeostasis through regulated uptake of protein-rich interstitial fluid into draining lymphatic vessels and transport of the drained lymphatic fluid into the blood

Supported by a grant (SC-5120; to G.Y.K.) from Stem Cell Research Center of the 21st Century Frontier Research Program and by a Korea Science Engineering Foundation grant funded by the Ministry of Education, Science and Technology, Korea [R2009-0079390 (to G.Y.K.) and R31-2008-000-10071-0 (to G.Y.K.)].

Accepted for publication June 22, 2009.

Supplemental material for this article can be found on *http://ajp.amjpathol.org*.

Address reprint requests to Gou Young Koh, M.D., Ph.D., Department of Biological Sciences, Korea Advanced Institute of Science and Technology, 373-1, Guseong-dong, Daejeon 305-701, Republic of Korea. E-mail: gykoh@kaist.ac.kr.

vasculature via collecting lymphatic vessels.[9] In addition, lymphatic vessels have roles in lipid absorption, antigen presentation, tumor metastasis, and wound healing.[10–16] Lymphatic vessels beneath the peritoneum, particularly lymphatic vessels on the peritoneal side of the muscular region of diaphragm, provide the central route for draining peritoneal fluid.[2,17,18]

Lymphatic vessels on the peritoneal side of the diaphragm are largely attenuated but well designed for fluid absorption with extremely flattened and broad lumina (also called lacunae), which are connected with openings between mesothelial cells covering the peritoneal surface.[2,19] In comparison, lymphatic vessels on the pleural side of diaphragm are tubular, like other lymphatic vessels.[20,21] There are seven to nine parallel lymphatic strips on each hemisphere (sterno-costal muscular region) of the peritoneal side of diaphragm, and these lymphatic vessels are directly connected to the tubular lymphatic vessels on the pleural side by transmural lymphatic branches.[20–22] Therefore, the peritoneal fluid absorbed by lymphatic lacunae is directly transported into the lymphatic vessels on the pleural side. In contrast, there are few lymphatic vessels in the central tendon region of the diaphragm. However, little is known about relationship between the structural and functional changes of diaphragmatic lymphatic vessels and peritoneal illnesses.

Our understanding of the molecular and cellular regulation of new lymphatic vessel formation, "lymphangiogenesis," has greatly advanced in recent years.[10] Among lymphangiogenic growth factors, the roles of vascular endothelial growth factor (VEGF)-C and VEGF-D (VEGF-C/D) and their lymphatic vessel-specific receptor VEGF receptor-3 (VEGFR-3) are specific and essential in lymphangiogenesis.[10] In addition, VEGF-A and its receptors play additional roles in lymphangiogenesis in certain pathological conditions.[10,11] Moreover, proinflammatory cytokine-induced activation of macrophages is closely involved in pathological lymphangiogenesis in tracheal mucosa and cornea by reciprocal interactions with the VEGF-C/D-VEGFR-3 system.[12–15] However, the relationship between proinflammatory cytokine-induced activation of macrophages and pathological changes of diaphragmatic lymphatic vessels during peritonitis is unknown.

In this study, we investigated how acute inflammatory peritonitis affects the diaphragmatic lymphatic vessels structurally and functionally and what roles are played by activated macrophages in this situation. To generate a peritonitis model, we administered lipopolysaccharide (LPS; endotoxin) directly into the peritoneal cavity of mouse. LPS is a well-known cell wall component of most Gram-negative bacteria and acts as a potent initiator of inflammation.[23,24] Interestingly, mice with LPS-induced peritonitis displayed aberrant lymphangiogenesis, lymphatic remodeling, and lymphatic dysfunction in the diaphragm. We have defined the underlying mechanisms and the responsible molecules by using specific blocking agents to reveal the roles of critical effector cells and molecules. Our results show that $CD11b^+$ macrophages have an important role in LPS-induced aberrant lymphangiogenesis and lymphatic dysfunction in the diaphragm.

Materials and Methods

Animals and Treatment

Specific pathogen-free FVB/N and C57BL/6J mice were purchased from The Jackson Laboratory (Bar Harbor, ME) and bred in our pathogen-free animal facility. GFP^+ mice (C57BL/6J genetic background) were a gift from Dr. Masaru Okabe (Osaka University, Osaka, Japan). Animal care and experimental procedures were performed under approval from the Animal Care Committees of Korea Advanced Institute of Science and Technology. All experiments were conducted in FVB/N mice, otherwise specifically indicated. Five or 25 μg of LPS (from *Escherichia coli* 0111:B4; Sigma-Aldrich, St. Louis, MO) in 200 μl of PBS was injected daily into the peritoneal cavity of 8-week-old male mice. As a control, 200 μl of PBS was injected in the same manner. To block VEGF-C and VEGF-D, mice were treated with a single i.v. injection of 1×10^9 plaque-forming units of adenovirus-encoding soluble VEGFR-3 (Ad-sVEGFR-3)[25] one day before the LPS (5 μg/day for 7 days) administration. As a control, 1×10^9 plaque-forming units of Ad-LacZ was injected in the same manner.

Histological and Morphometric Analysis

On the indicated days after the treatments, mice were anesthetized by intramuscular injection of a combination of anesthetics (80 mg/kg ketamine and 12 mg/kg xylazine). The indicated tissues were fixed by 1% paraformaldehyde in PBS and whole-mounted or cryoembedded and sectioned. Whole-mounted tissues and cryosections were incubated for 1 hour at room temperature with blocking solution containing 5% goat serum (Jackson ImmunoResearch Laboratories, West Grove, PA) in PBST (0.3% Triton X-100 in PBS). After blocking, the samples were incubated overnight at 4°C with one or more of the following primary antibodies: (a) for lymphatic vessels, rabbit anti-lymph vessel endothelial hyaluronan receptor (LYVE)-1 polyclonal antibody (1:1000; Upstate Biotechnology, Lake Placid, NY) and rat anti-LYVE-1 monoclonal antibody (clone Han-1, 1:1000; Aprogen, Daejeon, Korea); rabbit anti-Prox1 polyclonal antibody (1:1000; ReliaTech, Braunschweig, Germany); (b) for blood vessels, hamster anti-PECAM-1 antibody (clone 2H8, 1:1000; Chemicon International, Temecula, CA); (c) for macrophages, rat anti-CD11b antibody (clone M1/70, 1:1000; BD Pharmingen, San Diego, CA); rat anti-mouse F4/80 antibody (clone Cl:A3-1, 1:1000; Serotec, Oxford, UK), rat anti-mouse Gr-1 antibody (clone RB6-8C5, 1:1000; BD Pharmingen), hamster anti-mouse CD11c antibody (clone N418, 1:1000; Serotec), and rat anti-mouse CD45R/B220 antibody (clone RA3-6B2a, 1:1000; BD Pharmingen); and (d) for an assay of proliferation, rabbit anti-phosphohistone H3 polyclonal antibody (1:500; Upstate Biotechnology). After several washes in PBST, the samples were incubated for 3 hours at room temperature with the following secondary antibodies. For 3,3′-diaminobenzidine (DAB) immunostaining, samples were incubated with horseradish peroxidase-conjugated anti-rat IgG an-

tibody (Jackson ImmunoResearch Laboratories) or horseradish peroxidase-conjugated anti-rabbit IgG antibody (Amersham, Piscataway, NJ) and developed with DAB substrate kit (Vector Laboratories, Burlingame, CA) according to the manufacturer's instructions. For immunofluorescent staining, the samples were incubated with the following antibodies: fluorescein isothiocyanate (FITC)- or Cy5-conjugated anti-rat IgG antibody (1:1000; Jackson ImmunoResearch Laboratories); Cy3- or Cy5-conjugated anti-hamster IgG antibody (1:1000; Jackson ImmunoResearch Laboratories); and FITC- or Cy3-conjugated anti-rabbit IgG antibody (1:1000; Jackson ImmunoResearch Laboratories). For control experiments, the primary antibody was omitted or substituted with preimmune serum. DAB and fluorescent signals were visualized, and digital images were obtained using a Zeiss inverted microscope, a Zeiss ApoTome microscope, or a Zeiss LSM 510 confocal microscope equipped with argon and helium-neon lasers (Carl Zeiss). Morphometric analyses on the lymphatic vessels of diaphragm were made by ImageJ software (http://rsb.info.nih.gov/ij) or using Zeiss ApoTome microscope image analysis software (AxioVision; Carl Zeiss). Measurements of the density of the lymphatic vessels and the areas of $CD11b^+$ cells in diaphragms were made at three regions at peritoneal and pleural surfaces of muscle regions, or central tendon region, each 35.18 or 0.21 mm^2 in the area, with three to four mice per group. Numbers of Prox1 or PH3 immunopositivelymphatic endothelial cells (LECs) were counted at 3 regions, each 0.21 mm^2 in the immunopositive area, of the central tendon regions or muscular regions of diaphragms. Measurements of the density of the lymphatic and blood vessels in lymph nodes (LNs) were made on a whole field, each 0.17 mm^2 in the immunopositive area. Values were obtained per mm^2 and expressed as relative densities. In some instances, the sectioned tissues were stained with H&E or Masson's trichrome according to standard methods. To estimate the size of the LNs, we measured the length (L) and width (W) of each LN, then calculated the volume according to following equation: $4/3\pi \times L/2 \times W/2 \times (L + W)/4$.

Flow Cytometric Analyses of $CD11b^+$ Macrophages from Diaphragm

After anesthesia, diaphragms were harvested and dissected into small pieces by a microscissor, and the pieces were incubated with 5 ml of Hanks' balanced salt solution (Sigma-Aldrich) containing 0.2% collagenase type-II (Worthington) for 1 hour at 37°C. After inactivation of collagenase activity with bovine serum, the cell suspension was filtered through a 70-μm nylon filter (BD Biosciences) and centrifuged at 400 $\times$ *g* for 5 minutes. The filtered cells were incubated with Red Blood Cell lysing buffer (Sigma-Aldrich) for 5 minutes and washed with a FACS buffer (0.5% BSA and 0.01 M EDTA in PBS) and double-stained with perCP-cy5.5-conjugated rat anti-mouse CD11b and FITC-conjugated rat anti-mouse F4/80, FITC-conjugated rat anti-mouse Gr-1, PE-conjugated rat anti-mouse CD11c, or FITC-conjugated rat anti-mouse B220 (BD Biosciences) for 15 minutes at 4°C. Then the cells were analyzed by flow cytometry (FACSCalibur; BD Biosciences) using a Cell Quest software. A total of ~50,000 cells were counted per sample. Data were analyzed by using FlowJo software (Tree Star, Ashland, OR).

Bone Marrow Transplantation

Bone marrow cells (2×10^6) were harvested from the femurs and tibias of GFP^+ mice (C57BL/6J genetic background) by flushing with ice-cold Dulbecco's PBS (Sigma-Aldrich). The recipient mice (8-week-old C57BL/6J) were sublethally irradiated at a dose of 4.5 Gy with a gamma irradiator (Gammacell 3000; MDS Nordion, Canada). Bone marrow cells were then injected i.v. into the recipient mice 16 hours after irradiation. At 8 weeks after transplant, 5 μg of LPS was injected daily into the peritoneal cavity for 1 week. Flow cytometric analysis revealed that more than 90% of peripheral blood mononuclear cells were GFP^+ cells at this time point.

RT-PCR

At the indicated days after treatment, mice were anesthetized and diaphragms were harvested. To collect $CD11b^+$ macrophages from diaphragms, the attached cells were collected following the method as described in the flow cytometric analysis. After several washes of collected cells in cold PBS, the $CD11b^+$ macrophages were enriched by using anti-mouse CD11b antibody-coupled MicroBeads (Miltenyi Biotec) and a Magnetic Cell Sorter (MACS, Miltenyi Biotec) according to the manufacturer's instructions. Total RNA from the enriched $CD11b^+$ macrophages was extracted by using Total RNA Isolation System (Promega, Madison, WI) according to the manufacturer's instructions. Each cDNA was made with Reverse Transcription System (Promega), and semiquantitative PCR was performed with the appropriate primers (Table 1) with 30 cycles used for the PCR. Quantitative RT-PCR was performed with SYBR Premix Ex Taq (Takara, Japan) using the iCycler iQ5 Real-time PCR system (Bio-Rad, Hercules, CA) with the appropriate primers (Table 1) for 40 cycles.

Functional Assays for Lymphatic Drainage

On the indicated days after the LPS or PBS treatment, the mice were anesthetized, 300 μl of India ink (Pelikan, catalog no. 4001, Hannover, Germany) was injected into the peritoneal cavity, and the mice were kept on a warm pad in a supine position. At 15 minutes after injecting India ink, diaphragms were harvested, fixed with 1% paraformaldehyde in PBS and photographed. To determine a functional rate of lymphatic drainage of peritoneal large molecules into the sentinel LNs (SLNs) through diaphragmatic lymphatic vessels, 50 μl of Fluoresbrite (plain fluorescent YG microspheres, diameter, 2.0 μm; Polysciences, Washington, PA) diluted with 250 μl of PBS was injected into the peritoneal cavity of mice, and the

Table 1. Primers for Semiquantitative RP-PCR and Quantitative Real-Time RT-PCR

VEGF-A*	Forward	5′-GAGAGCAGAAGTCCCATGAAGTG-3′
	Reverse	5′-CTTTCCGGTGAGAGGTCTGG-3′
VEGF-A**	Forward	5′-GCTGTACCTCCACCATGCCAAG-3′
	Reverse	5′-CGCACTCCAGGGCTTCATCG-3′
VEGF-C*	Forward	5′-GACATGTCCAACAAACTATGTGTGG-3′
	Reverse	5′-CTGTTACCATGGTCCCACAGAG-3′
VEGF-D*	Forward	5′-CCGGGAGATCTCATTCAGCACC-3′
	Reverse	5′-GCACAATAACTCATGAGCATTGCCC-3′
Angiopoietin-1*	Forward	5′-CAGTGGCTGCAAAAACTTGA-3′
	Reverse	5′-TCCGCACAGTCTCGAAATGG-3′
Angiopoietin-2*	Forward	5′-CCGCTATGAAGTTCCTCTCTGC-3′
	Reverse	5′-CTGCTATGCAATGGTGTCTCTC-3′
Interleukin-6*	Forward	5′-GTCCAAGCAGAGCTCTGTCATTG-3′
	Reverse	5′-GATGGTCTTGGTCCTTAGCCAC-3′
Interleukin-1β*	Forward	5′-GAAGAGCCCATCCTCTGTGACTC-3′
	Reverse	5′-GTCCTGACCACTGTTGTTTCCCAG-3′
TNF-α*	Forward	5′-CCCACGTCGTAGCAAACCAC-3′
	Reverse	5′-CACAGAGCAATGACTCCAAAGTAG-3′
β-Actin*	Forward	5′-CCCGCCACCAGTTCGCC-3′
	Reverse	5′-GAGGGAGAGCATAGCCCTCG-3′
GAPDH**	Forward	5′-AGGTCGGTGTGAACGGATTTG-3′
	Reverse	5′-TGTAGACCATGTAGTTGAGGTCA-3′

* Primers for semiquantitative RT-PCR.
** Primers for quantitative real-time RT-PCR.
TNF, tumor necrosis factor; GAPDH, glyceraldehyde-3-phosphate dehydrogenase.

mice were kept on a warm pad in a supine position. At 15 and 60 minutes after injecting the microspheres, two SLNs and diaphragms were harvested and fixed with 1% paraformaldehyde in PBS or embedded with tissue freezing medium. The fluorescent microspheres were visualized in the midsectioned SLNs and diaphragm after immunostaining for lymphatic vessels.

Macrophage Depletion

For systemic depletion of macrophages, mice were treated with i.p. injections of clodronate liposome (25 mg/kg for every 3 days) as described previously.[26,27] As a control, empty control liposome was injected in the same manner.

Cecal Ligation-Puncture Model

Mice were anesthetized by intramuscular injection of the combination of anesthetics as described above, and a 1-cm midline incision was made to expose the cecum. The cecum was ligated with a 4-0 black silk suture and punctured with an 18-gauge needle. The cecum was squeezed to push a small amount of cecal contents from the punctured site into the peritoneal cavity, then was returned to the peritoneal cavity.[28] Sham operation without cecal ligation-puncture (CLP) was performed as a control.

Statistics

Values are presented as mean ± SD. Significant differences between means were determined by analysis of variance followed by the Student-Newman-Keuls test. Statistical significance was set at $P < 0.05$.

Results

LPS Induces a Increase Lymphatic Density and Remodeling in the Diaphragm

Because lymphatic vessels in the diaphragm play a primary role in absorbing peritoneal fluid and in removing pathogens,[2,3,20–22] we focused our experiments on characterizing the LPS-induced changes to lymphatic vessels in the diaphragm. LPS (5 μg) was administered daily into the i.p. cavity of 8-week-old mice. At 1 week after the LPS treatment, whole-mounted diaphragms were immunostained for LECs by using a specific marker, LYVE-1.[29] The daily administration of LPS gradually increased lymphatic densities on the peritoneal side muscular region, the pleural side muscular region, and the pleural side central tendon region in a time-dependent manner (Figures 1 and 2, A and B). In the peritoneal side muscular region, the lymphatic strips were widened and enlarged, and typical lymphatic patterning was disrupted over time (Figure 2A). In the pleural side muscular region, randomly oriented lymphatic branching increased over time (Figure 2A). In the pleural side, central tendon region, lymphatic connections, and networks increased over time (Figure 2A). Daily administration of 25 μg of LPS for 1 week did not further increase the lymphatic density on the pleural side muscular region and pleural side central tendon regions, but it did further widen and enlarge the lymphatic strips on the peritoneal side muscular region (Figure 2, A and B). Immunofluorescent staining of sagittal sections of the diaphragm in the mice treated with 5 μg of LPS for 1 week displayed enlarged lymphatic vessels in the peritoneal side muscular region and enlarged and connected lymphatic vessels mainly in the pleural side

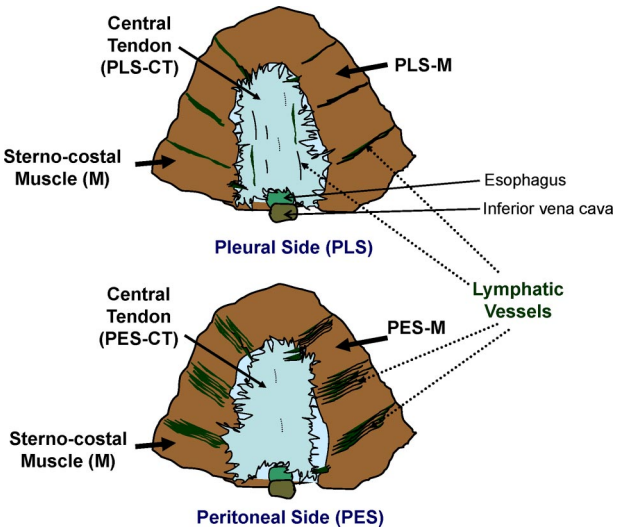

Figure 1. Schematic diagrams and nomenclature of the diaphragm in mouse. Two views of the diaphragm showing the peritoneal side (PES) and pleural side (PLS). The sterno-costal muscle (M) and central tendon (CT) separate the peritoneal cavity from the pleural cavity. Several parallel lymphatic strips are present in the PES-M region, whereas several tubular lymphatic vessels are present in the PLS-M region. A few disconnected lymphatic vessels are present in the PLS-CT region.

central tendon region compared with the mice treated with PBS (Figure 2C). Discontinuation of the daily administration of 5 μg of LPS normalized the macroscopic lymphatic structure, patterning, and density within 2 weeks (Supplemental Figure S1, see *http://ajp.amjpathol.org*). Thus, LPS induced a substantial increase in lymphatic density and remodeling in the diaphragm, and this remodeling was time-dependent, dose-dependent, and reversible.

LPS-Induced Lymphatic Remodeling Occurs Mainly through LEC Proliferation

To investigate whether the observed changes in lymphatic density and remodeling resulted from proliferation of LECs or by extension or hypertrophy, we used double-immunostaining for LYVE-1/PH3 (nuclear protein of dividing cells) and LYVE-1/Prox1 (specific transcriptional factor for LECs).[30] The number of PH3$^+$ LECs markedly increased in the enlarged lymphatic vessels of peritoneal side muscular region of the mice treated with LPS (5 μg/day for 1 week) (LPS versus PBS, ~4.6-fold; Figure 3, A and B). Similarly, the number of Prox1$^+$/LYVE-1$^+$ LECs markedly increased in the pleural side central tendon region of the mice treated with LPS (LPS versus PBS, ~2.4-fold; Figure 3, A and C). Moreover, the number of sprouts greatly increased in the lymphatic vessels of the pleural side central tendon region of the mice treated with LPS (LPS versus PBS, ~17.2-fold; Figure 3, A and D). These data indicated that the LPS-induced lymphatic density and remodeling mainly resulted from the proliferation of LECs and active sprouting, which are the major cellular processes of lymphangiogenesis.[7,8,10,11]

CD11b$^+$ Macrophages Are Associated with Growing Lymphatic Vessels

Previous studies[31,32] have shown that macrophages and neutrophils are massively recruited into the peritoneal cavity during inflammation. In this study, H&E and Masson's trichrome staining and immunofluorescent detection of CD11b$^+$ cells in the diaphragm of mice treated with LPS (5 μg/day for 1 week) revealed massive accumulation of inflammatory cells, including macrophages and neutrophils, and moderate fibrosis in the peritoneal

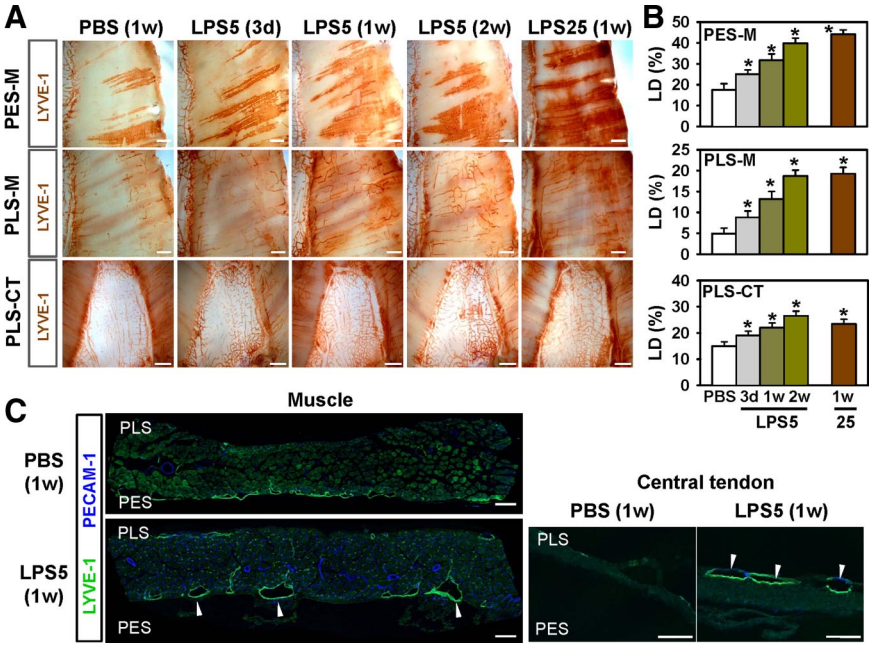

Figure 2. LPS induced increased lymphatic density and remodeling in the diaphragm. On the indicated days after daily i.p. injections of PBS, or 5 or 25 μg of LPS (LPS5 or LPS25), diaphragms were harvested and whole mounted (**A**) or sectioned (**C**). The diaphragms were immunostained with anti-LYVE-1 antibody (for lymphatic vessels) and anti-PECAM-1 antibody (for lymphatic and blood vessels), and visualized with DAB (**A**) or fluorescent (**C**) staining. **A:** Lymphatic vessels in the PES-M, PLS-M, and PES-CT regions of the diaphragms are shown. Scale bars, 1 mm. Note that there are gradual increases in lymphatic densities, diameters, random branching, and network formation in the diaphragms of the LPS-treated mice over time. **B:** Densities of LYVE-1$^+$ lymphatic vessels were measured, and values are presented as a percentage, with each measured total area counted as 100%. All bars represent mean ± SD (n = 4–5 mice). *$P < 0.05$ versus PBS. **C:** LPS induces lymphatic enlargements (**white arrows**) in the PES-M and PLS-CT regions. Scale bars, 100 μm.

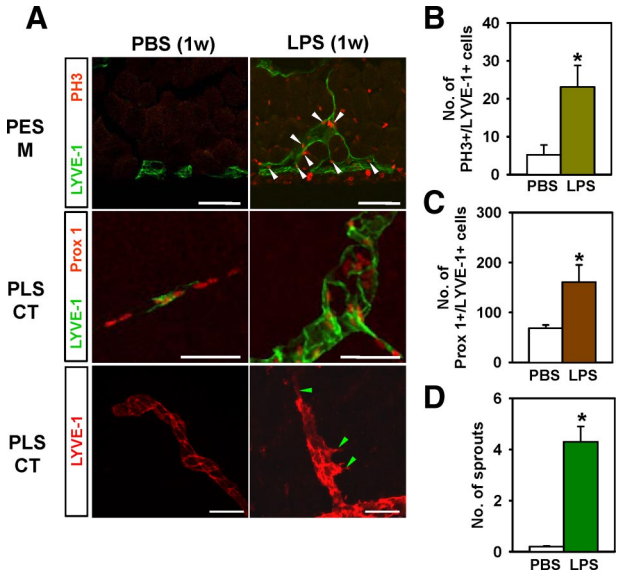

Figure 3. LPS induced active proliferation and sprouting of LECs. One week after daily i.p. injections of PBS or 5 μg of LPS, diaphragms were harvested, sectioned, or whole mounted, and immunostained with anti-LYVE-1 (Han-1) and anti-PH3 or anti-Prox1 antibodies. **A:** The PES-M and PLS-CT regions are shown. **White arrowheads** indicate LYVE-1$^+$/PH3$^+$ LECs, and **green arrowheads** indicate lymphatic sprouts. Scale bars, 50 μm. **B–D:** Numbers of LYVE-1$^+$/PH3$^+$ cells were counted in 0.21 mm^2 of the PES-M region, and numbers of LYVE-1$^+$/Prox1$^+$ cells and sprouts were counted in 0.21 and 0.42 mm^2 of the CT region. All bars represent mean ± SD (n = 4–5 mice). *P < 0.05 versus PBS.

side muscular region (Figure 4, A and B). In comparison, no notable changes were detected in the same regions of the PBS-treated mice. Noticeably, CD11b$^+$ cells were mainly attached to the lymphatic vessels of the peritoneal side muscular region in the LPS-treated mice (Figure 4B). In this region, immunostaining showed many cells positive for both F4/80 (macrophage surface maker) and Gr-1 (neutrophil and macrophage surface maker), but few cells positive for both CD11c (dendritic cell surface maker) and B220 (B-lymphocyte surface marker) (Figure 4C). Flow cytometric analyses revealed that approximately 20 to 25% of the CD11b$^+$ cells in the diaphragmatic lymphatic vessels were F4/80$^+$ or Gr-1$^+$ macrophages, whereas a negligible number of the CD11b$^+$ cells were CD11c$^+$ or B220$^+$ cells (Figure 4D). These data suggest that the CD11b$^+$ cells are macrophages, and these cells are closely associated with the diaphragmatic lymphatic vessels in LPS-induced peritonitis. To clarify the origin of the macrophages in the diaphragmatic lymphatic vessels, 8-week-old mice (C57BL/6J) received GFP$^+$ bone marrow transplantation and then were treated with LPS for 1 week beginning 8 weeks after transplantation. Most CD11b$^+$ macrophages in the diaphragmatic lymphatic vessels were GFP$^+$ (Figure 5A). In fact, flow cytometric analysis revealed that 84.2 ± 4.7% (n = 4) of the CD11b$^+$ macrophages were GFP$^+$ cells (data not shown). These data suggest that most of the macrophages were derived from bone marrow through circulation, and few were derived from resident macrophages from the i.p. cavity. To determine whether bone marrow-derived cells act as "lymphatic endothelial progenitor cells"[15] to form new LECs during the LPS-induced lymphangiogenesis and lymphatic remodeling, we carefully examined the colocalization of LYVE-1 and GFP by confocal microscopy.

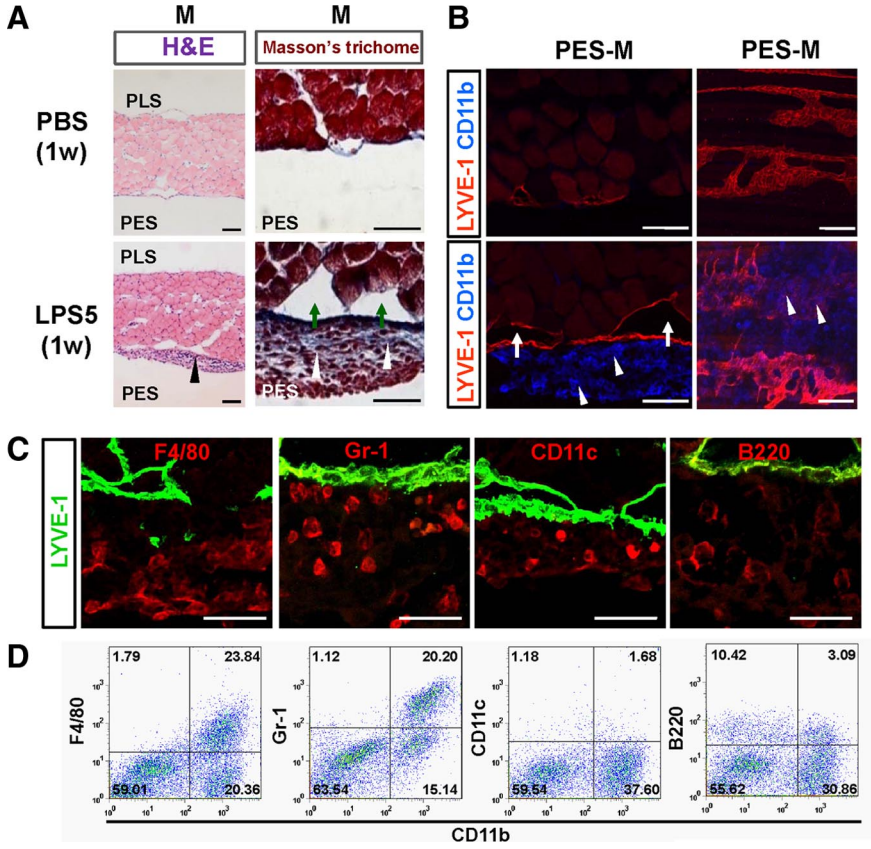

Figure 4. CD11b$^+$ macrophages were closely associated with diaphragmatic lymphatic vessels in LPS-treated mice. One week after daily i.p. injections of PBS or 5 μg of LPS (LPS5), diaphragms were harvested, sectioned, or whole mounted and stained with H&E and Masson's trichrome (**A**) or immunostained with anti-LYVE-1 and anti-CD11b antibodies (**B**). Note that the LPS-treated mice have blue-stained fibrotic tissues containing inflammatory cells (**white arrowheads**) in the mesothelium and enlarged lymphatic vessels (**green arrows**) between the inflamed mesothelium and the PES-M region. In particular, CD11b$^+$ macrophages (**white arrowheads**) are massively accumulated around the lymphatic vessels of the PES-M region in the LPS-treated mice. Scale bars, 100 μm. **C:** Double immunofluorescent staining for LYVE-1 and F4/80, Gr-1, CD11c, or B220 in the PES-M of the LPS-treated mice. Scale bars, 20 μm. **D:** Flow cytometric analyses for CD11b and F4/80, Gr-1, CD11c, or B220 in the inflammatory cells derived from the PES-M of the LPS-treated mice. Three independent experiments showed similar findings.

However, on the basis of our rigorous observations, we found no GFP^+ cells in the LECs of the diaphragm (Figure 5B). Thus, the LPS-induced increased lymphatic density and remodeling are induced by lymphangiogenesis from pre-existing lymphatic vessels, not by transdifferentiation of bone marrow-derived cells.[10,11,15]

Major Role of $CD11b^+$ Macrophage-Derived Lymphangiogenic VEGFR-3 Ligands in LPS-Induced Lymphangiogenesis and Lymphatic Remodeling in the Diaphragm

These observations led us to examine whether $CD11b^+$ macrophages express lymphangiogenic factors that drive LPS-induced lymphangiogenesis and lymphatic remodeling. A series of semiquantitative and quantitative real-time RT-PCR assays was performed on the $CD11b^+$ macrophages isolated from LPS-treated mice. The expression levels of lymphangiogenic factors VEGF-A_{164}, VEGF-A_{120}, VEGF-C, VEGF-D, angiopoietin-2, and proinflammatory cytokines tumor necrosis factor-α, interleukin-1β, and interleukin-6 increased in a time-dependent manner (Figure 6, A and B). The expression level of one lymphangiogenic factor, angiopoietin-1, was not changed by the LPS treatment (Figure 6, A and B). Among the lymphangiogenic factors that increased, the increases in VEGF-C and -D were the largest. Thus, the $CD11b^+$ macrophage-derived lymphangiogenic factors VEGF-C/D may play a major role in LPS-induced lymphangiogenesis and lymphatic remodeling in the diaphragm in a paracrine manner. To address the role of VEGF-C/D derived from $CD11b^+$ macrophages in the LPS-induced lymphangiogenesis and lymphatic remodeling in the diaphragm, mice were treated with 1×10^9 plaque-forming units of Ad-sVEGFR-3.[25] Compared with the mice treated with Ad-LacZ, the mice treated with Ad-sVEGFR-3 displayed markedly reduced density, branching, and sprouting of lymphatic vessels in the peritoneal side-muscle (PES-M) region without a significant change in $CD11b^+$ macrophage infiltration (Figure 6, C and D), indicating that $CD11b^+$ macrophage-driven VEGF-C/D are the main mediators of LPS-induced aberrant lymphangiogenesis.

LPS-Induced Lymphatic Vessels Are Dysfunctional Because of Massive Attachment of Macrophages

To compare the drainage function of the diaphragmatic lymphatic vessels, we injected India ink i.p. into PBS- and LPS-treated mice. At 15 minutes after injection in the PBS-treated mice, most lymphatic vessels in the peritoneal side muscular region, but not in the central tendon area, of the diaphragm contained ink (Figure 7A). In contrast, most India ink in the LPS-treated mice was absorbed into the lymphatic vessel-associated macrophages instead of the lymphatic vessels in the peritoneal side muscular region of the diaphragm (Figure 7B). Only some of large lymphatic vessels that had taken up ink were seen in the pleural side muscular region in the LPS-treated mice (Figure 7B). These phenomena were confirmed in sagittal sections of the diaphragm (Figure 7C). In the LPS-treated mice, most ink was detected in the macrophages attached to the peritoneal side muscular region, whereas in the PBS-treated mice, most ink was detected in the pleural side muscular region and transmural regions of the diaphragm. Then we further examined drainage of peritoneal large particles to the SLNs. In the normal diaphragm, lymphatic fluid containing large molecules collects and drains into the right lymphatic duct via the cranial mediastinal LN (CMLN) and tracheal lymphatic trunk.[33,34] As a secondary pathway, it is transported to the thoracic duct via the caudal MLN.[33,34] Because the CMLN is relatively accessible and visible by simple microsurgery, we analyzed the drainage rate by detection of fluorescent microspheres (diameter, 2.0 μm) in the CMLN at 15 and 60 minutes after i.p. injection. In the PBS-treated mice, most of the microspheres were transported to the CMLN through the diaphragmatic lymphatic vessels (Figure 7, D and E). In contrast, the drainage rate of the microspheres in the LPS-treated mice was significantly slower than that of the PBS-treated mice at both time points (Figure 7, D and E). In the LPS-treated mice, most of the microspheres were trapped in the lymphatic vessel-associated macrophages of the peritoneal side muscular region (Figure 7, F and G). This phenomenon was confirmed by flow cytometry (Supplemental Figure S2, see *http://ajp.amjpathol.org*).

LPS Increases the Size of SLNs and Increases Their Lymphatic but Not Blood Vessel Density

To test whether LPS alters lymphatic vessels in SLNs, we examined the sizes and lymphatic and blood vessel densities of the two SLNs, the CMLN (lymphatic drainage from the abdominal cavity through diaphragmatic lymphatic vessels) and the mesenteric LN (lymphatic drainage directly from mesenteric lymphatic vessels), after daily i.p. administration of 5 or 25 μg of LPS. The LPS increased the sizes of both SLN in a dose-dependent manner, but the ratio of increase in the CMLN was greater than that in the mesenteric LN (Figure 8, A and C). In both SLNs, the lymphatic vessel densities and, to the lesser extent, blood vessel densities increased in a dose-dependent manner (Figure 8, B, D, and E).

Clodronate Liposome Treatment Partially Reduces LPS-Induced Changes in Diaphragmatic Lymphatic Vessels

On the basis of the aforementioned observations, we examined the role of macrophages in LPS-induced dysfunctional lymphangiogenesis by using a specific depletion agent, clodronate liposome[26,27] (25 mg/kg every 3 days i.p. from day 0 of the LPS or PBS treatment). As a control, an equal volume of control liposome was administered into mice in the same manner. The clodronate liposome treatment efficiently depletes macrophages in all organs of the abdominal cavity by inducing selective

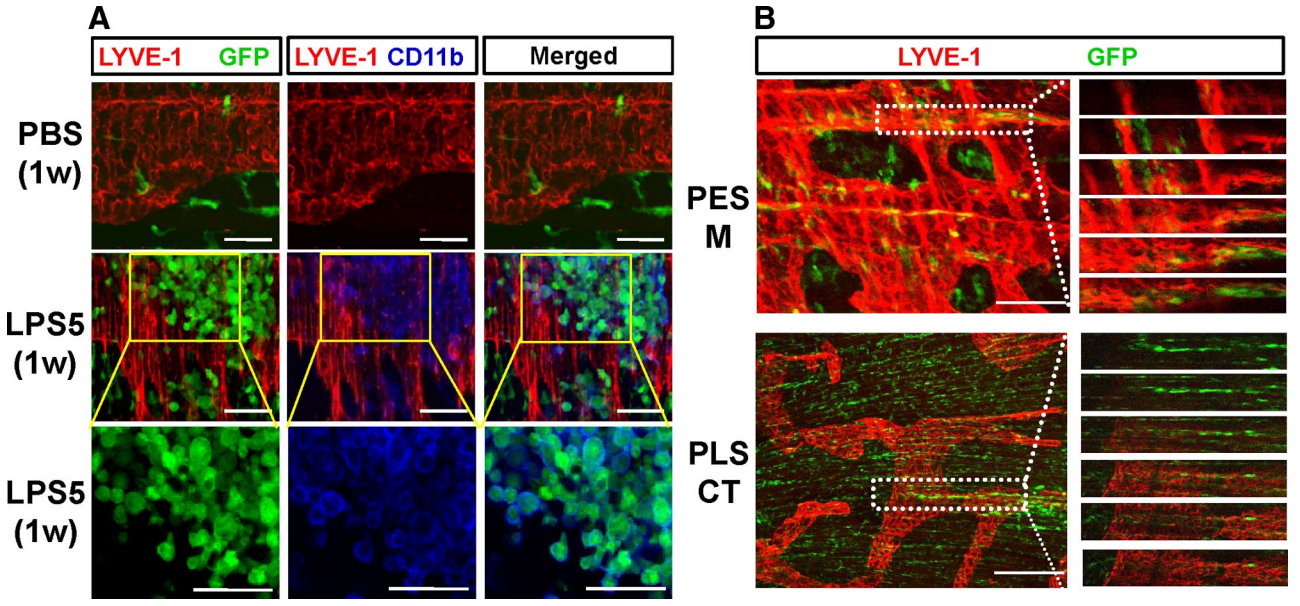

Figure 5. Most CD11b$^+$ macrophages were derived from bone marrow-derived macrophages, and bone marrow-derived circulating cells were not transdifferentiated into LECs. Mice received bone marrow transplants from GFP$^+$ mice; 8 weeks later, they were treated with daily i.p. injections of PBS or 5 μg of LPS (LPS5) for 1 week. Diaphragms were harvested, whole mounted, and immunostained with anti-LYVE-1 and anti-CD11b antibodies. **A:** Lymphatic vessels, CD11b$^+$ macrophages, and bone marrow-derived GFP$^+$ cells in the PES-M region are shown. The **lower panels** are higher magnifications of the **middle panels** (**insets**) after omission of LYVE-1 staining. Note that 80~90% of the accumulated CD11b$^+$ macrophages are GFP$^+$ cells. **B:** Some bone marrow-derived GFP$^+$ cells in the PES-M and PLS-CT look like LYVE-1$^+$ LECs (the white dotted rectangles in the **left panels**), but sequential dissected images (**right panels**) from the white dotted rectangles reveal no GFP$^+$/LYVE-1$^+$ cells in the PES-M and PLS-CT, indicating that bone marrow-derived GFP$^+$ cells are not transdifferentiated into LECs in the diaphragm during LPS-induced lymphangiogenesis. Scale bars, 50 μm.

apoptosis of macrophages (data not shown). The density and structure of lymphatic vessels, the CD11b$^+$ macrophage population, and India ink absorption to the lymphatic vessels in the diaphragm of the control liposome plus PBS- and clodronate liposome plus PBS-treated mice were identical to those of the PBS-treated mice (Figure 9, A and B). In comparison, mice treated with control liposome plus LPS displayed increased lymphatic density and remodeling, massive attachment of CD11b$^+$ macrophages to the lymphatic vessels, moderate fibrosis, preferential uptake of India ink into macrophages, and impaired ink drainage in the diaphragm (Figure 9, A and B). However, the clodronate liposome treatment markedly abolished the LPS-induced lymphatic density, sprouts and remodeling, and massive attachment of CD11b$^+$ macrophages in the peritoneal side muscular

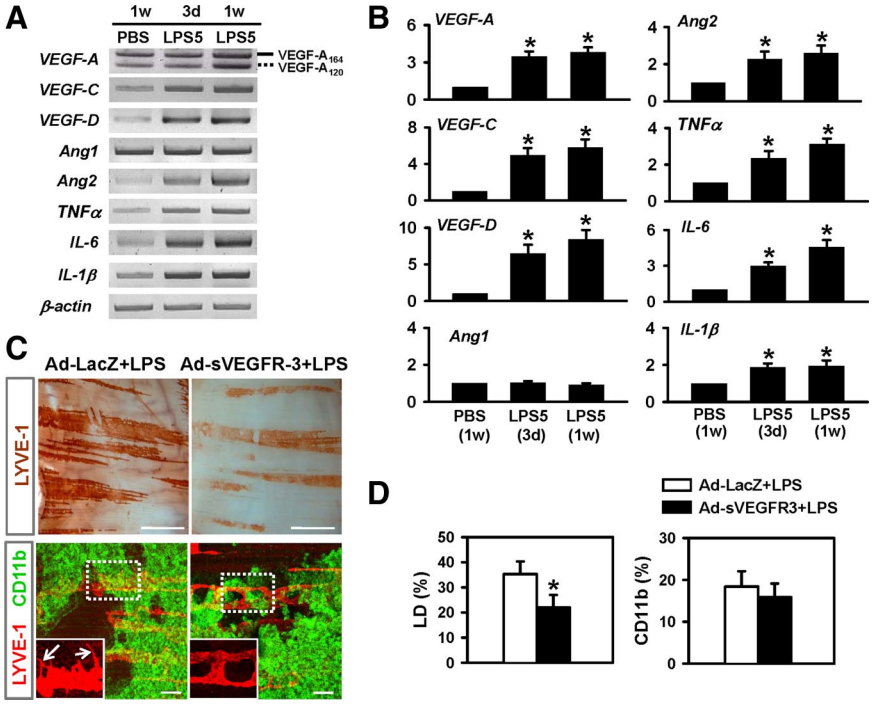

Figure 6. Paracrine lymphangiogenic role of CD11b$^+$ macrophages. **A** and **B:** Semiquantitative (**A**) and quantitative real-time (**B**) RT-PCR comparisons of VEGF ligands and cytokines in enriched CD11b$^+$ macrophages from the diaphragms of mice treated with PBS for 1 week [PBS (1w)] or with 5 μg of LPS for 3 days [LPS5(3 days)] or 1 week [LPS5(1w)]. Solid line, VEGF-A_{164}; dotted line, VEGF-A_{120}. **B:** The densitometric analyses are presented as the relative fold after normalization with glyceraldehyde-3-phosphate dehydrogenase. PBS (1w) is arbitrarily regarded as 1. Numbers represent the mean ± SD (n = 3–4). *P < 0.05 versus P (1w). **C** and **D:** The mice were treated with a single i.v. injection of 1 × 10^9 plaque-forming units of Ad-LacZ or Ad-sVEGFR-3 one day before the start of daily i.p. injections LPS (5 μg/day for 7 days). At 1 week later, diaphragms were harvested, whole mounted, and immunostained with anti-LYVE-1 (brown or red) and anti-CD11b (green) antibodies (**C**). The lymphatic vessels in the dotted rectangular areas are highly magnified (**insets**). **Arrows** indicate lymphatic sprouts. Scale bars, 100 μm. **D:** Densities of LYVE-1$^+$ lymphatic vessels and areas of CD11b$^+$ cells were measured, and values are presented as a percentage, with each measured total area counted as 100%. All bars represent mean ± SD (n = 4–5 mice). *P < 0.05 versus Ad-LacZ + LPS.

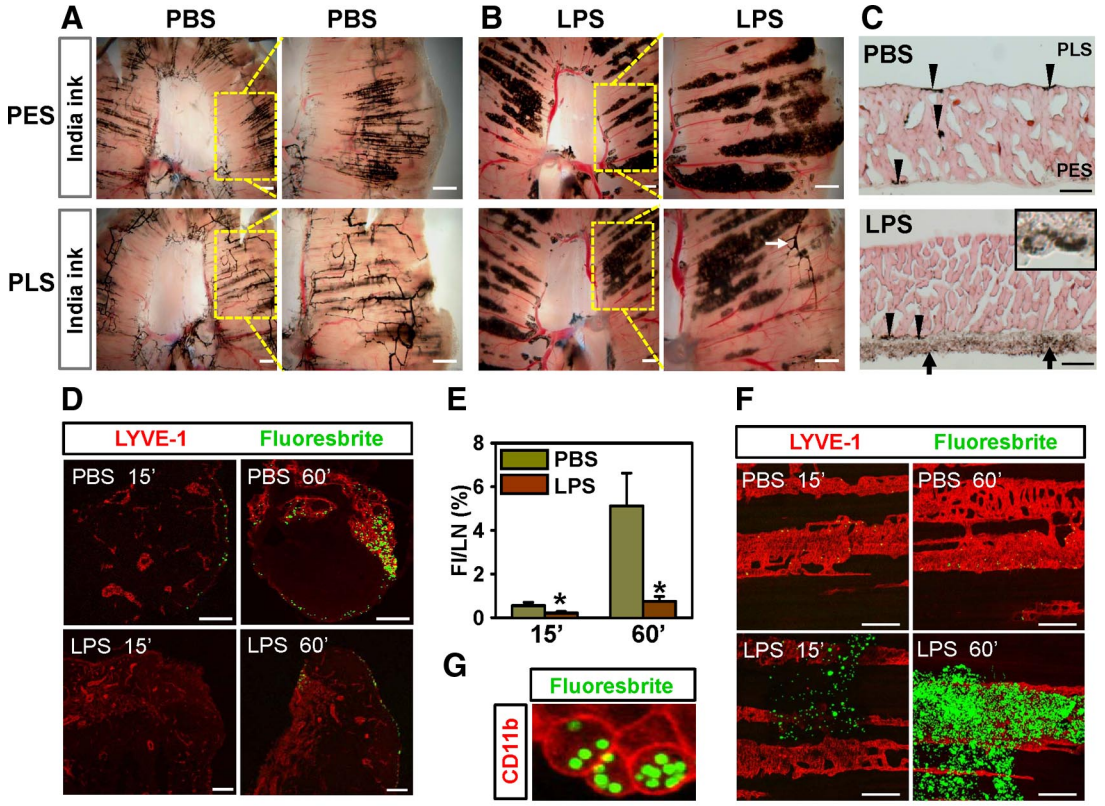

Figure 7. LPS induced defective peritoneal fluid drainage as a result of massive attachment of macrophage to the diaphragmatic lymphatic vessels. **A–C:** One week after daily i.p. injections of PBS (**A**) or 5 μg of LPS (**B**), mice were given an i.p. injection of India ink. At 15 minutes after the injection, both sides of the diaphragms were photographed. Each **right panel** shows a magnified image of yellow dotted-lined square of each **left panel**. Note that in the PBS-treated mice, most ink is absorbed into the diaphragmatic muscular lymphatic vessels, whereas in the LPS-treated mice, most ink is absorbed into the lymphatic-associated macrophages. Scale bars, 1 mm. **C:** The diaphragms were sagittally sectioned and H&E stained. **Arrowheads** indicate ink-containing lymphatic vessels. Higher magnification (**inset**) shows that macrophages in the fibrotic tissue (**arrows**) contain India ink at the peritoneal side of the mesothelium. Scale bars, 200 μm. **D–G:** PBS- and LPS-treated mice were challenged with an i.p. injection of fluorescent microspheres. At 15 and 60 minutes after injection, the CMLN and the diaphragm are harvested, fixed, sectioned, or whole mounted and immunostained with anti-LYVE-1 antibody. **D:** Absorbed fluorescent microspheres and lymphatic vessels in CMLN are shown. Scale bars, 200 μm. **E:** Fluorescence intensity (FI) is quantified and presented as percentage of total area of the sectioned LNs. Bars represent mean ± SD ($n = 4$ mice). $^*P < 0.05$ versus PBS. **F:** Fluorescent microspheres and lymphatic vessels in the PES-M region are shown. Note that most fluorescent microspheres are trapped in the lymphatic-associated macrophages in the LPS-treated mice. Scale bars, 200 μm. **G:** Fluorescent microspheres containing CD11b$^+$ macrophages in the LPS-treated mice at 60 minutes after microsphere injection.

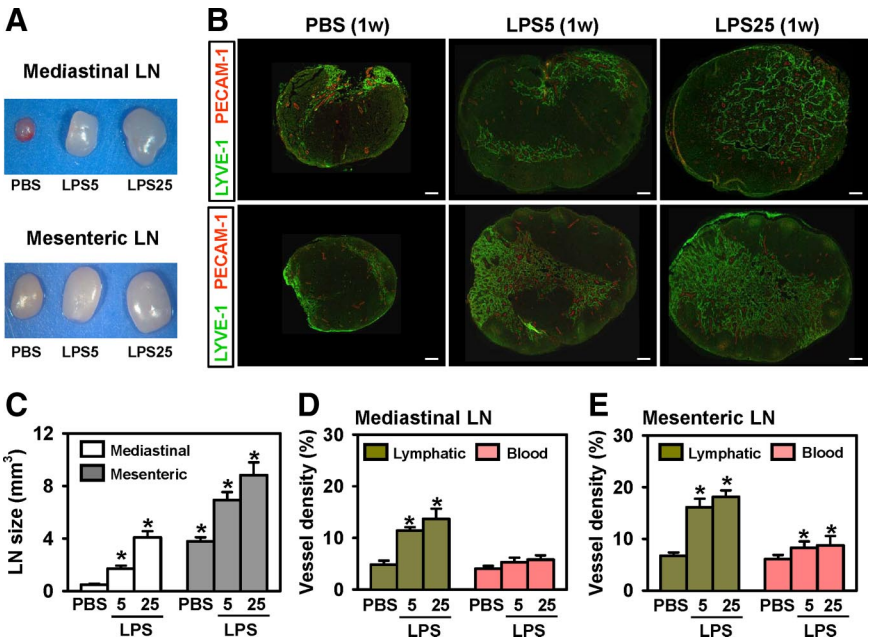

Figure 8. Intraperitoneal LPS increased the sizes and lymphatic densities of SLNs. One week after daily i.p. injections of PBS or 5 or 25 μg of LPS (LPS5 or LPS25), CMLN and MLN were harvested, measured, sectioned through the middle, and immunostained with anti-LYVE-1 (for lymphatic vessels) and anti-PECAM-1 (for blood and lymphatic vessels). **A** and **B:** Differences in LN sizes and lymphatic densities are shown. **C–E:** Sizes of the LN were measured (mm^3), and LYVE-1$^+$ lymphatic densities and PECAM-1$^+$ blood vessel densities were measured and presented as percentage of total area of the sectioned lymph nodes. All bars represent mean ± SD ($n = 3$–4 mice). $^*P < 0.05$ versus PBS. Scale bars, 100 μm.

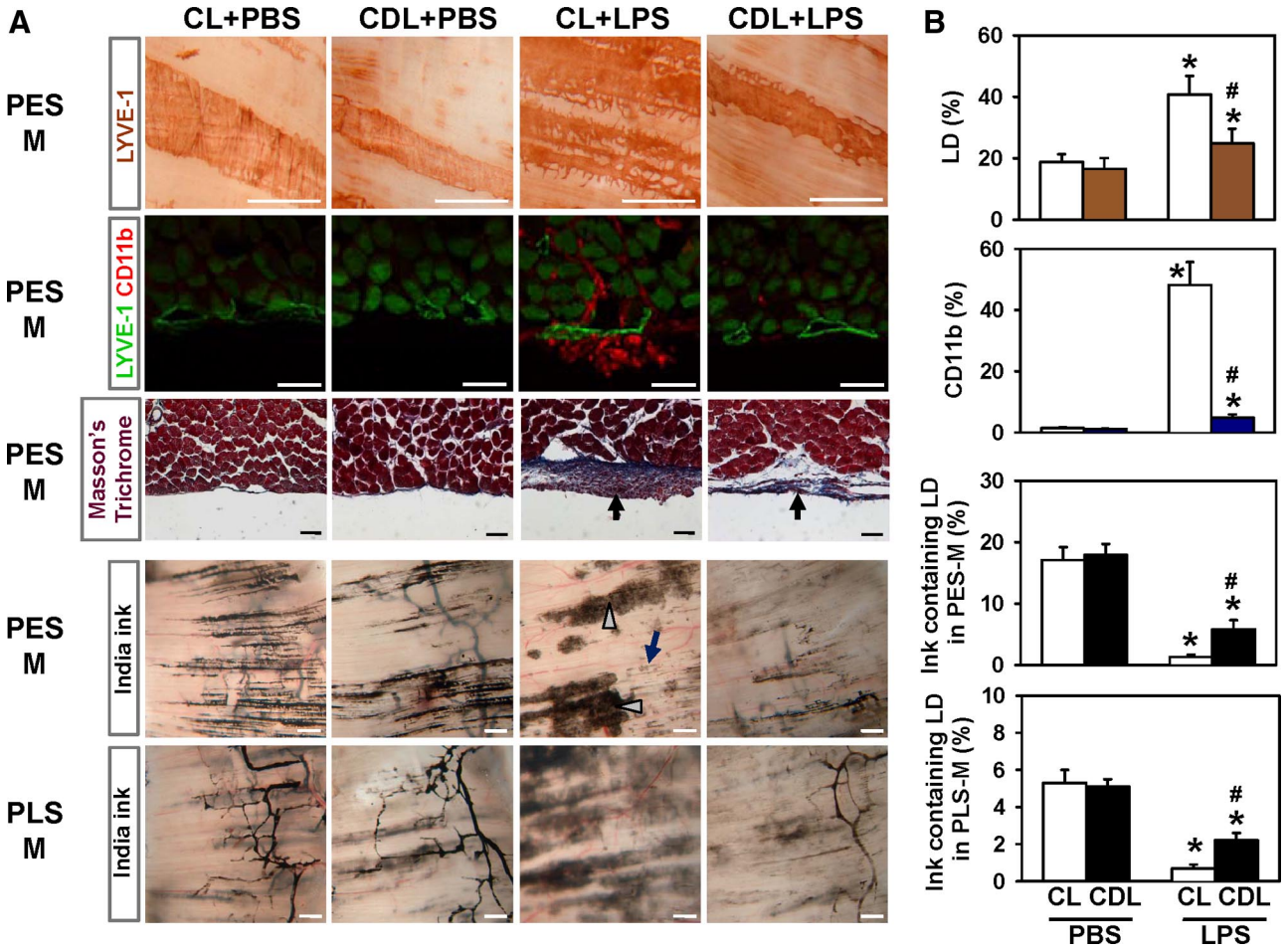

Figure 9. Clodronate liposome treatment partially reduced LPS-induced changes in diaphragmatic lymphatic vessels. The mice had daily i.p. injections of PBS or 5 μg of LPS and were treated with clodronate liposome (25 mg/kg; CDL) or control liposome (25 mg/kg; CL) every 3 days beginning the same day as the start of PBS or LPS treatment. One week later, diaphragms were harvested, whole mounted or sectioned, and LYVE-1$^+$ lymphatic vessels or CD11b$^+$ macrophages of the PES-M and PLS-M regions were immunostained and visualized by DAB (**first row panels**) or fluorescent dye (**second row panels**) and stained with Masson's trichrome (**third row panels**). Note that the thickness of the blue-stained fibrotic tissue in the PES-M region of the mice treated with clodronate liposome + LPS is thinner than that in mice treated with CL + LPS (**arrows**). Another set of mice was challenged with an i.p. injection of India ink; at 15 minutes after the injection, the PES-M and PLS-M regions of the diaphragms were photographed (**fourth** and **fifth row panels**). Note that most ink was absorbed into the lymphatic vessel-associated macrophages (**gray arrowheads**) instead of the lymphatic vessels (**dark-blue arrow**) in the PES-M region of the mice treated with CL + LPS. Scale bars, 50 μm (rows 2 and 3) and 500 μm (rows 1, 4, and 5). **B:** The area densities of LYVE-1$^+$ lymphatic vessels, CD11b$^+$ cells, and ink-containing lymphatic vessels in the PES-M and PLS-M were measured, and the values are presented as percentages, with each measured total area counted as 100%. All bars represent mean ± SD (n = 4–5 mice). *$P < 0.05$ versus CL + PBS or clodronate liposome (CDL) + PBS; #$P < 0.05$ versus CL + LPS.

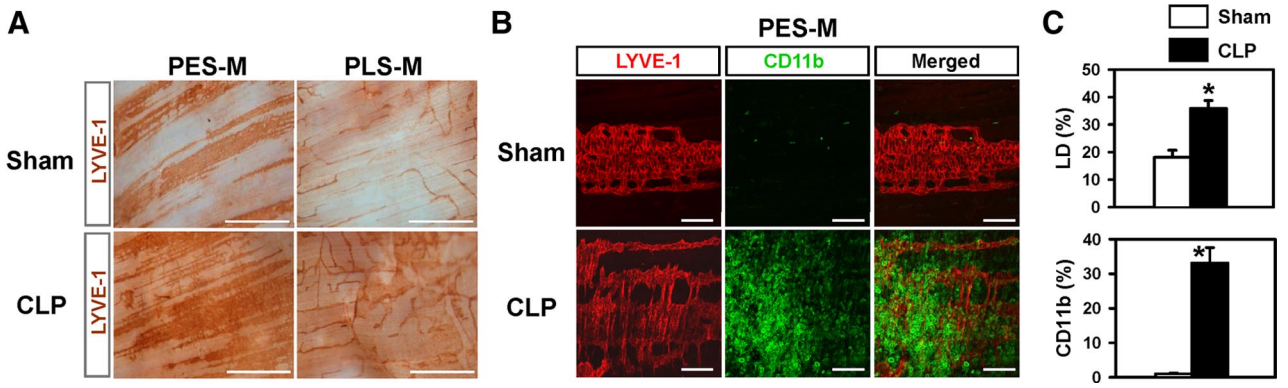

Figure 10. CLP peritonitis model produced similar changes in the diaphragmatic lymphatic vessels. **A** and **B:** Three days after the CLP or sham operation, diaphragms were harvested and whole mounted. LYVE-1$^+$ lymphatic vessels and CD11b$^+$ macrophages in the PES-M or PLS-M regions were immunostained and visualized by DAB (**A**) or fluorescent dye (**B**). Scale bars, 1 mm (**A**) and 100 μm (**B**). Note that there are increased lymphatic densities and branching, and markedly accumulated CD11b$^+$ macrophages in the lymphatic vessels of the PES-M region in the CLP-operated mice compared with the sham-operated mice. **C:** Densities of LYVE-1$^+$ lymphatic vessels and areas of CD11b$^+$ cells were measured, and values are presented as a percentage, with each measured total area counted as 100%. All bars represent mean ± SD (n = 4–5 mice). *$P < 0.05$ versus Sham.

region (Figure 9, A and B). It also caused a moderate reduction of fibrosis in the peritoneal side muscular region and partial but significant restoration of ink drainage to the lymphatic vessels in both the peritoneal side muscular region and pleural side muscular regions (Figure 9, A and B). Because the clodronate liposome treatment could not completely abolish the inflammatory fibrosis in the peritoneal side muscular region, drainage through diaphragmatic lymphatic vessels may not be completely restored. Taken together, the macrophage depletion could attenuate LPS-induced lymphangiogenesis and lymphatic remodeling, and it could partially rescue LPS-induced lymphatic drainage dysfunction in the diaphragm.

CLP Peritonitis Causes Similar Changes in Diaphragmatic Lymphatic Vessels

To mimic a clinically relevant peritonitis model, we generated the CLP-induced peritonitis model. Most mice die around 5 to 7 days after the CLP operation. Therefore, we examined the mice at 3 days after the operation. In this model, lymphatic density and sprouts were markedly increased, and $CD11b^+$ macrophages were greatly accumulated in the lymphatic vessels in the peritoneal side muscular region (Figure 10, A–C). In contrast, the lymphatic vessels and number of $CD11b^+$ macrophages in the sham-operated mice were almost identical to those in the PBS-treated mice.

Discussion

In this study, we showed that the LPS-induced peritonitis mouse model displayed aberrant and dysfunctional lymphangiogenesis in the diaphragm. LPS-induced peritonitis induced profound and dynamic changes in lymphatic vessels of the diaphragm, including increased density and enlargement, random branching, and increased sprouts, connections, and network formation. These effects varied from region to region but were time-dependent, dose-dependent, and reversible. Moreover, the responses in the lymphatic vessels were much more than the responses in the blood vessels. Thus, the diaphragmatic lymphatic vessels are highly responsive to LPS-induced inflammation. Our immunohistochemical data provided compelling evidence that the LPS-induced lymphatic density and remodeling mainly resulted from proliferation of LECs and active sprouting from pre-existing lymphatic vessels, which are the major cellular processes of lymphangiogenesis.[7,8,10,11] To evaluate whether bone marrow-derived cells act as lymphatic endothelial progenitor cells,[15] to form LECs in the diaphragmatic lymphatic vessels during LPS-induced lymphangiogenesis and lymphatic remodeling, we carefully examined the bone marrow-derived cells in the LPS-induced growing lymphatic vessels by confocal microscopy. However, we found no bone marrow-derived cells in the LECs of the diaphragm, indicating that the LPS-induced lymphangiogenesis is not derived from transdifferentiation of bone marrow-derived cells.[10,11,15] To see whether a more clinically relevant peritonitis model would display similar changes in the diaphragmatic lymphatic vessels, we developed a CLP-induced peritonitis model. Because the CLP-induced peritonitis mouse model exhibited findings similar to those observed in the LPS-induced peritonitis model, it is possible that human patients with Gram-negative bacterial peritonitis may also have dysfunctional lymphangiogenesis and lymphatic remodeling in the diaphragm.

Because macrophage activation is closely involved in inflammation-induced lymphangiogenesis,[12–15,35] we investigated the interaction between macrophages and diaphragmatic lymphatic vessels at the histological and molecular levels in the LPS-treated mice. Histological analyses revealed that $CD11b^+$ macrophages were closely associated with the diaphragmatic lymphatic vessels in LPS-induced peritonitis. Moreover, $CD11b^-$ macrophages and other types of leukocytes, including neutrophils, could be associated with the diaphragmatic lymphatic vessels in LPS-induced peritonitis.

These associated macrophages and other types of leukocytes could induce lymphangiogenesis through secretions of lymphangiogenic growth factors in a paracrine manner.[16,36,37] To clarify the role of $CD11b^+$ macrophages in LPS-induced lymphangiogenesis, we performed RT-PCR analyses in the enriched $CD11b^+$ macrophages from the LPS-induced inflamed diaphragm, a blocking experiment with Ad-sVEGFR-3, and macrophage depletion experiments with clodronate liposome. These experiments revealed that the $CD11b^+$ macrophage-derived lymphangiogenic factors VEGF-C/D may play a major role in LPS-induced lymphangiogenesis and lymphatic remodeling in the diaphragm in a paracrine manner.

To monitor the drainage function of the diaphragmatic lymphatic vessels, we measured the absorption rate of India ink from the peritoneal cavity to the diaphragmatic lymphatic vessels. In LPS-induced peritonitis, there was impaired Indian ink drainage to the lymphatic vessels of the peritoneal side muscular region because of massive attachment of macrophages and inflammatory fibrosis. These observations led us to further examine the peritoneal drainage of large particles (fluorescent microspheres; diameter, 2.0 μm) to the SLN. Similarly, most of the fluorescent microspheres were trapped in the lymphatic vessel-associated macrophages of the peritoneal side muscular region. Thus, the LPS-induced lymphatic vessels displayed impaired drainage for peritoneal fluid and particles, mostly because of massive attachment of macrophages to diaphragmatic lymphatic vessels and fibrotic tissue in the peritoneal side muscular region. Moreover, it is possible that the large amount of attached macrophages and other types of leukocytes may also block the mesothelial stomata at the entrances to the lymphatic vessels in the peritoneal side muscular region of the diaphragm, and this would cause an additional physical barrier to the drainage of peritoneal fluid and particles.

What brings about the massive attachment of $CD11b^+$ macrophages to the LPS-induced inflamed diaphrag-

matic lymphatic vessels? We recently found that, during LPS-induced inflammation, the diaphragmatic lymphatic vessel is a major tissue in the production of chemokines through the Toll-like receptor-4 for macrophage recruitment and attachment.[37] Thus, secretion and changes in the lymphatic vessels themselves may be responsible for this effect.

Our results also revealed that the overall amount of tracer transported from the diaphragm to the SLN was less in the LPS-treated mice compared with the PBS-treated mice, although the size of an SLN was larger and the lymphatic vessel density was higher in the LPS-treated mice compared with the PBS-treated mice. These findings are quite different from those for LPS-induced skin inflammation and its SLN.[16] The main reason for this unique characteristic in the inflamed diaphragm could be the physical blockage of lymphatic vessels in the peritoneal side muscular region by massive attachment of macrophages and inflammatory fibrosis. In agreement with this idea, the impaired function of lymphatic drainage in the diaphragm was partially rescued when we specifically depleted macrophages in all organs, including the abdominal cavity, by inducing selective apoptosis of macrophages using clodronate liposome. However, although depletion of the i.p. macrophages, including $CD11b^+$ macrophages, in Gram-negative bacteria-induced peritonitis could provide beneficial effects for restoring lymphatic function in the diaphragm, it might be dangerous because such a therapy would abrogate the primary defense mechanism of macrophages against invading pathogens.

In conclusion, our findings reveal that $CD11b^+$ macrophages play an important role in i.p. LPS-induced aberrant lymphangiogenesis and lymphatic dysfunction in the diaphragm.

Acknowledgments

We thank Dr. Kari Alitalo for Ade-sVEGFR-3 and Ad-LacZ, Jin Yoon and Hyung-In Cho for technical assistance, and Jennifer Macke for critical reading of the manuscript.

References

1. Gandawidjaja L, Hau T: Anatomic, physiologic, bacteriologic and immunologic aspects of peritonitis. Acta Chirurgica Belgica 1997, 97:163–167
2. Tsilibary E, Wissig S: Light and electron microscope observations of the lymphatic drainage units of the peritoneal cavity of rodents. Am J Anat 1987, 180:195–207
3. Hall J, Heel K, Papadimitriou J, Platell C: The pathobiology of peritonitis. Gastroenterology 1998, 114:185–196
4. Ho H, Wu M, Yang Y: Peritoneal cellular immunity and endometriosis. Am J Reprod Immunol 1997, 38:400–412
5. Broche F, Tellado J: Defense mechanisms of the peritoneal cavity. Curr Opin Crit Care 2001, 7:105–116
6. Melichar B, Freedman R: Immunology of the peritoneal cavity: relevance for host-tumor relation. Int J Gynecol Cancer 2002, 12:3–17
7. Ji R: Lymphatic endothelial cells, lymphangiogenesis, and extracellular matrix. Lymphat Res Biol 2006, 4:83–100
8. Pepper M, Skobe M: Lymphatic endothelium: morphological, molecular and functional properties. J Cell Biol 2003, 163:209–213
9. Saladin K: Anatomy and physiology: the unity of form and function. The Lymphatic and Immune System. Edited by K Saladin. Boston, McGraw Hill, 2004, pp 799–835
10. Alitalo K, Tammela T, Petrova T: Lymphangiogenesis in development and human disease. Nature 2005, 438:946–953
11. Hong Y, Shin J, Detmar M: Development of the lymphatic vascular system: a mystery unravels. Dev Dyn 2004, 231:462–473
12. Baluk P, Tammela T, Ator E, Lyubynska N, Achen M, Hicklin D, Jeltsch M, Petrova T, Pytowski B, Stacker S: Pathogenesis of persistent lymphatic vessel hyperplasia in chronic airway inflammation. J Clin Invest 2005, 115:247–257
13. Maruyama K, Ii M, Cursiefen C, Jackson D, Keino H, Tomita M, Van Rooijen N, Takenaka H, D'Amore P, Stein-Streilein J: Inflammation-induced lymphangiogenesis in the cornea arises from CD11b-positive macrophages. J Clin Invest 2005, 115:2363–2372
14. Cursiefen C, Chen L, Borges L, Jackson D, Cao J, Radziejewski C, D'Amore P, Dana M, Wiegand S, Streilein J: VEGF-A stimulates lymphangiogenesis and hemangiogenesis in inflammatory neovascularization via macrophage recruitment. J Clin Invest 2004, 113:1040–1050
15. Kerjaschki D: The crucial role of macrophages in lymphangiogenesis. J Clin Invest 2005, 115:2316–2319
16. Kataru R, Jung K, Jang C, Yang H, Schwendener R, Baik J, Han S, Alitalo K, Koh G: Critical role of $CD11b^+$ macrophages and VEGF in inflammatory lymphangiogenesis, antigen clearance, and inflammation resolution. Blood 2009, 113:5650–5659
17. Nagy J: Lymphatic and nonlymphatic pathways of peritoneal absorption in mice: physiology versus pathology. Blood Purif 1992, 10:148–162
18. Abu-Hijleh M, Habbal O, Moqattash S: The role of the diaphragm in lymphatic absorption from the peritoneal cavity. J Anat 1995, 186:453–467
19. Tsilibary E, Wissig S: Lymphatic absorption from the peritoneal cavity: regulation of patency of mesothelial stomata. Microv Res 1983, 25:22–39
20. Azzali G: The lymphatic vessels and the so-called "lymphatic stomata" of the diaphragm: a morphologic ultrastructural and three-dimensional study. Microvasc Res 1999, 57:30–43
21. Shao X, Ohtani O, Saitoh M, Ohtani Y: Development of diaphragmatic lymphatics: the process of their direct connection to the peritoneal cavity. Arch Histol Cytol 1998, 61:137–149
22. Shinohara H: Lymphatic system of the mouse diaphragm: morphology and function of the lymphatic sieve. Anat Rec 1997, 249:6–15
23. Holst O, Ulmer A, Brade H, Flad H, Rietschel E: Biochemistry and cell biology of bacterial endotoxins. FEMS Immunol Med Microbiol 1996, 16:83–104
24. Tobias P, Tapping R, Gegner J: Endotoxin interactions with lipopolysaccharide-responsive cells. Clin Infect Dis 1999, 28:476–481
25. Makinen T, Jussila L, Veikkola T, Karpanen T, Kettunen M, Pulkkanen K, Kauppinen R, Jackson D, Kubo H, Nishikawa S: Inhibition of lymphangiogenesis with resulting lymphedema in transgenic mice expressing soluble VEGF receptor-3. Nat Med 2001, 7:199–205
26. Zeisberger S, Odermatt B, Marty C, Zehnder-Fjällman A, Ballmer-Hofer K, Schwendener R: Clodronate-liposome-mediated depletion of tumour-associated macrophages: a new and highly effective anti-angiogenic therapy approach. Br J Cancer 2006, 95:272–281
27. Seiler P, Aichele P, Odermatt B, Hengartner H, Zinkernagel R, Schwendener R: Crucial role of marginal zone macrophages and marginal zone metallophils in the clearance of lymphocytic choriomeningitis virus infection. Eur J Immunol 1997, 27:2626–2633
28. Corral J, Yelamos J, Hernandez-Espinosa D, Monreal Y, Mota R, Arcas I, Minano A, Parrilla P, Vicente V: Role of lipopolysaccharide and cecal ligation and puncture on blood coagulation and inflammation in sensitive and resistant mice models. Am J Pathol 2005, 166:1089–1098
29. Banerji S, Ni J, Wang S, Clasper S, Su J, Tammi R, Jones M, Jackson D: LYVE-1, a new homologue of the CD44 glycoprotein, is a lymph-specific receptor for hyaluronan. J Cell Biol 1999, 144:789–801
30. Wigle J, Oliver G: Prox1 function is required for the development of the murine lymphatic system. Cell 1999, 98:769–778
31. Leak L: Interaction of mesothelium to intraperitoneal stimulation. I. Aggregation of peritoneal cells. Lab Invest 1983, 48:479–491
32. Knudsen E, Iversen P, van Rooijen N, Benestad H: Macrophage-dependent regulation of neutrophil mobilization and chemotaxis dur-

ing development of sterile peritonitis in the rat. Eur J Haematol 2002, 69:284–296
33. Abernethy N, Chin W, Hay J, Rodela H, Oreopoulos D, Johnston M: Lymphatic removal of dialysate from the peritoneal cavity of anesthetized sheep. Kidney Int 1991, 40:174–181
34. Shibata S, Hiramatsu Y, Kaseda M, Chosa M, Ichihara N, Amasaki H, Hayakawa T, Asari M: The time course of lymph drainage from the peritoneal cavity in beagle dogs. J Vet Med Sci 2006, 68:1143–1147
35. Maruyama K, Asai J, Ii M, Thorne T, Losordo D, D'Amore P: Decreased macrophage number and activation lead to reduced lymphatic vessel formation and contribute to impaired diabetic wound healing. Am J Pathol 2007, 170:1178–1191
36. Jeon B, Jang C, Han J, Kataru R, Piao L, Jung K, Cha H, Schwendener R, Jang K, Kim K: Profound but dysfunctional lymphangiogenesis via vascular endothelial growth factor ligands from $CD11b^+$ macrophages in advanced ovarian cancer. Cancer Res 2008, 68:1100–1109
37. Kang S, Lee S, Kim K, Kim H, Memet S, Koh G: Toll-like receptor 4 in lymphatic endothelial cells contributes to LPS-induced lymphangiogenesis by chemotactic recruitment of macrophages. Blood 2009, 113:2605–2613